Predicting the Rupture Probabilities of Molecular Bonds in Series

Gregor Neuert,*† Christian H. Albrecht,* and Hermann E. Gaub*
*Ludwig-Maximilians-University Munich, Chair for Applied Physics & Center for Nano Science, Munich, Germany; and †Massachusetts Institute of Technology, Department of Physics, Cambridge, Massachusetts

ABSTRACT An assembly of two receptor ligand bonds in series will typically break at the weaker complex upon application of an external force. The rupture site depends highly on the binding potentials of both bonds and on the loading rate of the applied force. A model is presented that allows simulations of force-induced rupture of bonds in series at a given force and loading rate based on the natural dissociation rates $k_{R0,S0}$ and the potential width $\Delta x_{R,S}$ of the reference and sample bonds. The model is especially useful for the analysis of differential force assay experiments. This is illustrated by experiments on molecular force balances consisting of two 30-bp oligonucleotide duplexes where $k_{R0,S0}$ and $\Delta x_{R,S}$ have been determined for different single nucleotide mismatches. Furthermore, prediction of the rupture site of two bonds in series is demonstrated for DNA duplexes in combination with streptavidin/biotin and anti-digoxigenin/digoxigenin, respectively.

INTRODUCTION

Being a pivotal parameter in classical physics for centuries, force was not accessible on a molecular level in the biological sciences for a long time. Just recently single molecule experiments by means of force probe instruments such as atomic force microscope (AFM) (1–5), optical trap (6,7) magnetic tweezers (8,9), and biomolecular force probe (10,11) made it possible to investigate the mechanical properties of biological macromolecules (12,13). Receptor ligand bonds, which are commonly characterized by affinity measurements, have also been subject to single molecule force measurements. While affinities solely reflect the binding energy corresponding to the depth of the binding potential and therefore to the natural dissociation rate k_0, force measurements furthermore reveal an additional parameter, which is dependent on the unbinding pathway, the potential width Δx (14–16).

To derive Δx, a variety of force transducers like cantilevers (16–18), optical tweezers (19,20), and even biological membranes (11,15) have been employed to record force extension curves of receptor ligand bonds. Recently a fundamentally different approach to probe molecular forces has been introduced by our group (Fig. 1) (21–25). Here the microscopic force transducer is substituted by a single molecular bond, which is linked to the sample bond in series, thereby forming a molecular force balance. Upon application of a force at the ends of the balance, both bonds are probed simultaneously until the weaker one fails (21,22).

For highly symmetric combinations of sample (S) and reference (R) bonds, excellent sensitivity in terms of force differences is achieved, as demonstrated by detection of single nucleotide mismatches in DNA duplexes (21,22). However, due to the lack of a theoretical description, only ratios of discrimination have been assessed instead of quantitative differences in the natural dissociation rate of the reference k_{R0} and the sample k_{S0} bond as well as the potential width Δx_R and Δx_S.

Here we present a new theoretical approach for the analysis of force-induced unbinding of two bonds in series. By means of a reference bond where the binding potential is well characterized (known k_{R0} and Δx_R), we are able to calculate the dissociation rate k_{S0} and potential width Δx_S for an arbitrary sample bond based on the well-established Bell-Evans model for a given force and loading rate (14,26–28).

We apply this new analysis to experiments where small mutations have been introduced into a 30-bp oligonucleotide duplex. The results are compared to previous measurements on DNA oligonucleotides (17) and single chain antibodies performed by other groups (18). In general, we corroborate the finding of those earlier studies, namely that differences in k_{R0} of a receptor ligand bond are closely coupled to the potential width Δx_R (17,18).

Moreover, the theoretical model allows for predictions on alternative unbinding of any biological system where two bonds are probed in series. The model is particularly useful for simulations of force experiments (AFM, biomolecular force probe, and magnetic- and optical tweezers) where the sample is immobilized by affinity tags (7,20,29–34). Our approach allows one to predict whether a certain immobilization tag will survive the forces applied during the experiment or not.

MATERIALS AND METHODS

The principle of the molecular force balance

The technology of the molecular force balance has been described elsewhere in detail (22). Briefly, amino-labeled oligonucleotides are immobilized on an activated slide at their 3′-termini. Cy3 labeled oligonucleotides are now hybridized to the receptors, thereby forming a sample duplex. Subsequently biotin labeled oligonucleotides are hybridized to the sample, thereby forming a reference duplex. This results in a molecular balance as it is

Submitted November 6, 2006, and accepted for publication March 13, 2007.
Address reprint requests to H. E. Gaub, E-mail: gaub@lmu.de.
Editor: Jane Clarke.

0006-3495/07/08/1215/09 $2.00
doi: 10.1529/biophysj.106.100511

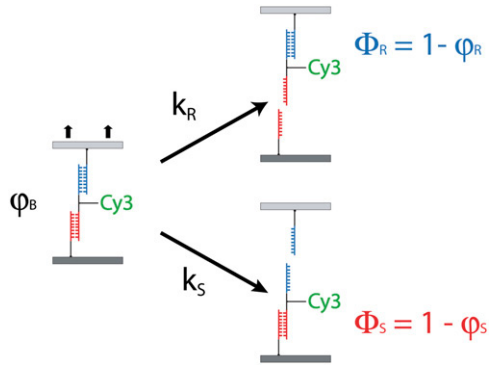

FIGURE 1 Experimental setup of the molecular force balance. A molecular force balance consisting of a reference bond (*blue*) and a sample bond (*red*) is immobilized between the chip surfaces in contact (*left*). Upon separation of the surfaces, force builds up in the balance until one of the bonds fails (*right*). The location of the fluorescent label after the separation indicates whether the reference or the sample bond was ruptured. The bond survival probability $\Phi_{R,S}$ depends on the rates of the reference bond k_R and the sample bond k_S.

depicted in Fig. 1. A stamp covered with streptavidin having an elevated microstructure is pressed onto the slide at this time. When the elevated area of the stamp makes contact with the slide, the biotinylated oligonucleotides will bind to the streptavidin. After the formation of biotin-streptavidin bond, the stamp is pulled away from the slide. The applied force will gradually increase until the reference duplex or the sample duplex ruptures, depending on which one is the weaker link. The Cy3-label of the middle oligonucleotide will therefore end up on the stamp when the sample duplex fails or on the slide when the reference duplex fails. Reading out the slide using a fluorescent scanner determines how much of the Cy3-oligonucleotide remained on the slide ($Cy3_{REM}$) in relation to the starting intensity $Cy3_{START}$. Thus, the normalized $Cy3_{REM}$ intensity reflects the survival probability of the sample duplex Φ_S when probed against a certain reference duplex Φ_R. In principle, Φ_S could also be deduced from the distribution of the Cy3-label between the stamp and the slide as described in Albrecht et al. (22); however, it is easier and more accurate to accomplish the readout just from the information on the slide. Therefore, in the following the stamp images are not used for the analysis.

The structure of the molecular balances is shown in Table 1.

Surfaces and instrumentation

The silicone stamp had 16 protruding contact areas which themselves were microstructured by 100 × 100 μm squares elevated by 5 μm. It was functionalized by treatment with epoxy-silane, subsequently coated with bifunctional amino-biotin-PEG and finally covered with streptavidin. The amino-oligonucleotides were labeled at the 3′-termini and attached to aldehyde-functionalized glass slides. After the hybridization of the other two oligonucleotides, stamp and slide were brought in contact by a piezoelectric element. The piezo allowed for precisely defined pulling velocities during surface separation (see (22) for details).

Analysis of fluorescence images

The image analysis procedure is shown in Fig. 2. The light-shaded DNA spot (Fig. 2 *A*) on a slide is depicted, where the fluorescence intensity of the Cy3-labeled oligo was measured. The area of contact between slide and stamp is equivalent to the darker squares, where the balances were probed and Cy3-labeled oligonucleotides were removed from the slide. The intensity of the darker squares corresponds to the remaining signal $Cy3_{REM}$. The light grid area is equivalent to the start intensity $Cy3_{START}$, where no contact was established between stamp and slide. The solid light-shaded line in Fig. 2 *A* indicates a region of interest (ROI-1) corresponding to the $Cy3_{REM}$ signal. Another two dashed black lines are enclosing the area of ROI-2, which corresponds to $Cy3_{START}$. The fluorescence intensity of the dark-shaded spot in Fig. 2 *B* represents biotin residues that have not coupled to the stamp, and which have been labeled by soluble AlexaFluor647-streptavidin after the Cy3-scan was performed. Accordingly, the AlexaFluor647 intensity of the dark squares reflects the coupling efficiency, as discussed in Albrecht et al. (22). Here (ROI-3) and (ROI-4) are enclosing the remaining biotin density $AF647_{REM}$ and the starting biotin density $AF647_{START}$.

For each of the 25 contact areas the mean intensities $Cy3_{REM}$, $Cy3_{START}$, $AF647_{REM}$, and $AF647_{START}$ have been determined. The degree of coupling was obtained by $AF647_{REM}/AF647_{START}$. To correct the Cy3-signal for the coupling efficiency, an offset of Cy3 was calculated from

$$Cy3_{offset} = Cy3_{REM} \times \frac{AF647_{REM}}{AF647_{START}}. \quad (1)$$

Finally, the survival probability of the sample duplex Φ_S was calculated from $Cy3_{REM}$, corrected for the coupling efficiency, and normalized to $Cy3_{START}$, according to Eq. 2:

TABLE 1 Four molecular force balances are depicted each comprising an amino-oligo (*top*), a Cy3-oligo (*middle*), and a biotin-oligo (*bottom*)

Dir.	Duplex	No.	Sequence
3′-5′	30PM	#66	NH2-20t-CTGCAGGAATTCGATATCAAGCTTATCGAT
5′-3′		#74	GACGTCCTTAAGCTATAGTTCGAATAGCTAc-17t-cATCGATAAGCTTGATATCGAATTCCTGCAGttttt-Cy3
3′-5′	30PM	#62	TAGCTATTCGAACTATAGCTTAAGGACGTC-20*t-Biotin
3′-5′	30GG	#66	NH2-20t-CTGCAGGAATTCGATATCAAGCTTATCGAT
5′-3′		#75	GACGTCCTTAAGGTATAGTTCGAATAGCTAc-17t-cATCGATAAGCTTGATATCGAATTCCTGCAGttttt-Cy3
3′-5′	30PM	#62	TAGCTATTCGAACTATAGCTTAAGGACGTC-20*t-Biotin
3′-5′	30CC	#66	NH2-20t-CTGCAGGAATTCGATATCAAGCTTATCGAT
5′-3′		#80	GACGTCCTTAACCTATAGTTCGAATAGCTAc-17t-cATCGATAAGCTTGATATCGAATTCCTGCAGttttt-Cy3
3′-5′	30PM	#62	TAGCTATTCGAACTATAGCTTAAGGACGTC-20*t-Biotin
3′-5′	29CC	#66	NH2-20t-CTGCAGGAATTCGATATCAAGCTTATCGAT
5′-3′		#86	_ACGTCCTTAACCTATAGTTCGAATAGCTAc-17t-cATCGATAAGCTTGATATCGAATTCCTGCAGttttt-Cy3
3′-5′	30PM	#62	TAGCTATTCGAACTATAGCTTAAGGACGTC-20*t-Biotin

Amino- and biotin-oligos are identical in all balances. Mutations are only introduced by single nucleotide exchanges (30GG, 30CC, 29CC) and a single nucleotide deletion (29CC) in the Cy3-oligonucleotides (underlined bases).

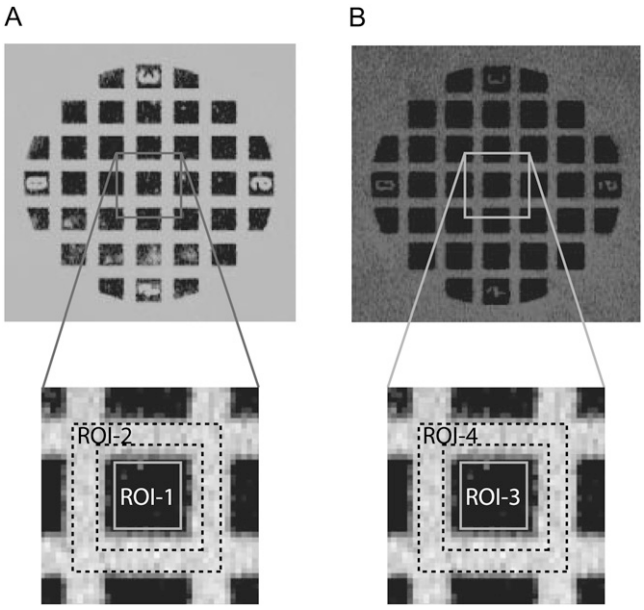

FIGURE 2 Fluorescent images are shown for the slide after separation of the stamp. (*A*) Image of the Cy3 fluorescent signal of a spot after separation. (*B*) The same spot after binding of fluorescent-streptavidin to the free biotin. Dark squares correspond to the contact area where the balances have ruptured. $Cy3_{START}$ intensity and $AF647_{START}$ intensity have been derived from ROI-1 and ROI-3, respectively. $Cy3_{REM}$ intensity and $AF647_{REM}$ intensity have been derived from ROI-3 and ROI-4 and correspond to the grid around one contact area.

$$\Phi_{S1-25} = \frac{Cy3_{REM} - Cy3_{offset}}{Cy3_{START} - Cy3_{offset}}. \quad (2)$$

Since not all of the contact areas showed a high homogeneity in terms of intensity and a good coupling efficiency, those $\Phi_{S1\text{-}25}$ values were selected that resulted in the minimal standard deviation (SD) for all of the measurement spots. This was the case for the following criteria: Coupling efficiency $> 85\%$; $SD(Cy3_{START}) < 14\%$; $SD(Cy3_{REM}) < 12\%$; $SD(AF647_{START}) < 15\%$; and $SD(AF647_{REM}) < 49\%$. According to those criteria, the SD for every kind of measurement spot (30PM, 30CC, 30GG, and 29CC) was $<5\%$, as indicated in Table 2.

Calculation of dissociation rates $k_{R0,S0}$ and the Gibb's free energy differences $\Delta G_{R,S}$

The Gibb's free energy difference $\Delta G_{R,S}$ for the DNA perfect match and mismatch duplexes was calculated by the computer program HyTher (Wayne State University, Detroit, MI; http://ozone3.chem.wayne.edu/cgi-bin/login/login/showLoginPage.cgi), which is based on the nearest-neighbor algorithm refined for mismatches by SantaLucia (36,37), for 150 mM Na^+, 25°C, and 100 nM of each oligonucleotide. The dissociation rate $k_{R0,S0}$ of the duplexes were then calculated from the equilibrium constant of dissociation

$$K_D = \frac{k_{R0,S0}}{k_{on}} = e^{\frac{\Delta G_{R,S}}{k_B T}}, \quad (3)$$

and with $k_{on} = 10^6\ M^{-1}\ s^{-1}$, based on the assumption that k_{on} is diffusion-limited and identical for all DNA duplexes (38).

TABLE 2 Summary of the input parameters for the simulations and the resulting potential width $\Delta x_{R,S}$ values

Duplex	Φ_S	$\Delta G_{R,S}$ [k_BT]	$k_{R0,S0}$ [s^{-1}]	$\Delta x_{R,S}$ [nm]
Reference	—	−45.02	2.82×10^{-14}	2.800
30PM	0.406 ± 0.016	−45.02	2.82×10^{-14}	2.834 ± 0.006
30GG	0.271 ± 0.010	−41.88	6.49×10^{-13}	2.612 ± 0.005
30CC	0.199 ± 0.010	−37.24	6.76×10^{-11}	2.228 ± 0.005
29CC	0.179 ± 0.009	−35.39	4.26×10^{-10}	2.072 ± 0.005

$\Delta G_{R,S}$ is the Gibbs free energy difference, $k_{R0,S0}$ is the natural dissociation rate, and Φ_S is the measured survival probability.

Determination of loading rate and rupture force

The loading rate r and the corresponding rupture force f of the balance were estimated from the applied velocity $v = 5$ nm/s, the polymer spacer length $L_0 = 30$ nm, dissociation rate $k_{R0} = 2.81 \times 10^{-14}\ s^{-1}$, and potential width $\Delta x_R = 2.8$ nm of the reference duplex, according to the model from Friedsam et al. (28).

Simulations

Each survival probability for the reference Φ_R and the sample duplex Φ_S was simulated by increasing the force f and keeping the loading rate $r_{0,1,2,3,4}$ fixed at the same time. Simulations and data fits were performed with Mathematica (Wolfram Research, Champaign, IL) and IGOR (WaveMetrics, Portland, OR).

RESULTS

Theoretical model

Despite the fact that a differential force assay is carried out on a large ensemble of molecular balances at the same time, each of the balances is probed individually without cooperative effects from neighboring molecules. Therefore, a single molecule approach is adequate for the theoretical description of the assay.

According to the experiments presented later, where the molecular balance comprises a constant reference duplex and a variable sample duplex, the goal of the simulation is to derive the survival probability Φ_S of the sample from the potential width Δx_S and the dissociation rate k_{S0} in a combination with a certain reference bond with Δx_R and k_{R0}.

To calculate Φ_S, the molecular force balance is modeled based on reaction rates, as shown in Fig. 1, where Φ_R and Φ_S indicate survival probabilities for the reference and sample duplex, respectively. According to Fig. 1, the time-dependent rupture probabilities can be expressed as a system of coupled ordinary differential equations, depending only on the dissociation rates k_R and k_S:

$$\frac{d\varphi_B(t)}{dt} = -(+k_R - k_S) \times \varphi_B(t), \quad (4A)$$

$$\frac{d\varphi_R(t)}{dt} = k_R \times \varphi_B(t), \quad (4B)$$

$$\frac{d\varphi_S(t)}{dt} = k_S \times \varphi_B(t). \quad (4C)$$

To solve Eqs. 4A–4C, the probabilities of $\varphi_B\ (t=0)=1$, $\varphi_R\ (t=0)=0$, and $\varphi_S\ (t=0)=0$ are used as boundary conditions at $t=0$ s when the bonds are just about to rupture. The association reaction is neglected based on the assumption that forced unbinding happens much faster than the association reaction. In contrast to the force balance experiment where intact bonds are detected by means of the fluorophore, the solution of the differential equations equals probabilities ($\varphi_R(t)$) and ($\varphi_S(t)$) corresponding to ruptured bonds. Therefore, the survival probabilities $\Phi_R(t)$ and $\Phi_S(t)$ of the intact bonds are calculated from

$$\Phi_R(t) = 1 - \varphi_R(t), \tag{5A}$$

$$\Phi_S(t) = 1 - \varphi_S(t), \tag{5B}$$

and plotted as a function of time in Fig. 3 *A*. Please note that all probability diagrams represent experiments on very large ensembles ($n \sim 10^9$) of molecular balances and not single molecule data.

To convert k_R and k_S into force-dependent rates, the Bell-Evans model for force-induced unbinding was applied to obtain

$$k_R(f) = k_{R0}(f=0) \times e^{f\cdot\Delta x_R/k_BT}, \tag{6A}$$

$$k_S(f) = k_{S0}(f=0) \times e^{f\cdot\Delta x_S/k_BT}, \tag{6B}$$

where $\Delta x_{R,S}$ is the distance between the bound and the transition state in a triangular binding potential and f is the external applied force. The constants k_{R0} and k_{S0} correspond to the natural dissociation rates in equilibrium, which were calculated from the free energy equilibrium constants K_D, as discussed above. The applied force tilts the binding potential and thus lowers the transition state energy by $f \times \Delta x_{R,S}$, causing the reference and sample bond to dissociate faster. The rate constants in Eq. 1 are therefore substituted by the force-dependent rates $k_R = k_R(f)$ and $k_S = k_S(f)$. An example for survival probability functions $\Phi_R(t, f)$ and $\Phi_S(t, f)$ for different external applied forces was plotted in Fig. 3 *A* over the logarithm of time. The timescale was normalized with respect to the time of dissociation of the reference bond at zero force $t_{R0} = k_{R0}^{-1}$. Since the experimentally accessible variables are the separation velocity v and force f, the loading rate r and the time were substituted by $r = df/dt$, as shown in Fig. 3 *B*. With this substitution, the final form of the differential equations is given in Eqs. 7A–7C and the solutions are plotted in Fig. 3 *B*:

$$\frac{d\varphi_B(f,r)}{df} = \left(\frac{-k_{R0}\times e^{f\cdot\Delta x_R/k_BT} - k_{S0}\times e^{f\cdot\Delta x_S/k_BT}}{r}\right)\times\varphi_B(f,r), \tag{7A}$$

$$\frac{d\varphi_R(f,r)}{df} = \frac{k_{R0}\times e^{f\cdot\Delta x_R/k_BT}}{r}\times\varphi_B(f,r), \tag{7B}$$

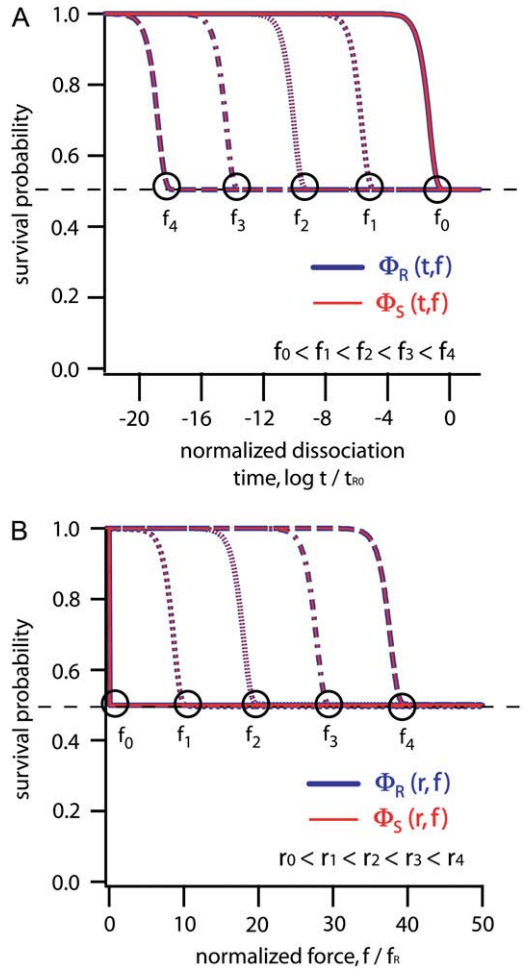

FIGURE 3 Solutions of the Eqs. 7A–7C are plotted for a symmetric balance with $t_{R0} = 1/k_{R0} = 3.55 \times 10^{13}$ s, $k_{R0,S0} = 2.82 \times 10^{-14}$ s^{-1}, and $\Delta x_{R,S} = 2.8$ nm. (*A*) Survival probabilities of the reference bonds (*blue*) and sample bonds (*red*) are plotted as function of the logarithm of the normalized dissociation time for rupture forces of $f_0 = 0$ pN, $f_1 = 10 \times f_R$, $f_2 = 20 \times f_R$, $f_3 = 30 \times f_R$, and $f_4 = 40 \times f_R$ with $f_R = k_BT/\Delta x_R = 1.48$ pN. (*B*) The same survival probabilities are plotted as shown in panel *A* as a function of normalized force f/f_R for loading rates $r_0 = 0$ pN/s, $r_1 = 4 \times 10^{-9}$ pN/s, $r_2 = 1.5 \times 10^{-4}$ pN/s, $r_3 = 4$ pN/s, and $r_4 = 1 \times 10^5$ pN/s. Black circles indicate the point where all balances are ruptured for different rupture forces $f_{0,\,1,\,2,\,3,\,4}$.

$$\frac{d\varphi_S(f,r)}{df} = \frac{k_{S0}\times e^{f\cdot\Delta x_S/k_BT}}{r}\times\varphi_B(f,r). \tag{7C}$$

Here, the survival probability of the sample Φ_S and the reference bond Φ_R were plotted as a function of normalized force f/f_R, with respect to the reference bond, where $f_R = k_BT/\Delta x_R$ is the characteristic force (10).

The experimentally acquired survival probability of the sample duplex Φ_S corresponds to the point where the dotted red line converges toward the solid red line in the following diagrams. In Fig. 3 *B* and the following diagrams, this point is highlighted by a black circle.

Simulations

In Fig. 4, *A–D*, the binding potentials and survival probabilities for different types of molecular balances are depicted in dependence of loading rates and rupture forces. Depending on the grade of asymmetry, the external force will bend the binding potential of the reference bond (*blue lines*) and the sample bond (*red lines*) to a different degree according to Eqs. 7*A*–7*C*. In particular, the reference bond is characterized by a Gibbs free energy difference of $-45.02\ k_BT$ and a potential width of 2.8 nm. With these two values, the binding potential and the potential width in Fig. 4 were normalized. Furthermore, the natural dissociation rate was calculated to $k_{R0} = 2.82 \times 10^{-14}\ s^{-1}$, using Eq. 3. The potential width of the reference bond Δx_R sets the characteristic force for the reference bond according to $f_R = 4.14$ pN/nm/2.8 nm = 1.48 pN.

In Fig. 4, *A–D*, left, the binding potential was tilted by $f \times \Delta x_R$. Here we applied five different forces of multiples of f_R: $f_0 = 0$ pN, $f_1 = 10 \times f_R$, $f_2 = 20 \times f_R$, $f_3 = 30 \times f_R$, and $f_4 = 40 \times f_R$. The simulations for the survival probability Φ_S as a function of the normalized force f/f_R were then performed at five different loading rates of $r_0 = 0$ pN/s, $r_1 = 4 \times 10^{-9}$ pN/s, $r_2 = 1.5 \times 10^{-4}$ pN/s, $r_3 = 4$ pN/s, and $r_4 = 1 \times 10^5$ pN/s (Fig. 4, *A–D*, *right*).

Perfectly symmetric balances

A balance where the reference and the sample bond are equal in terms of $\Delta x_{R,S}$ and $k_{R0,S0}$ could be considered as perfectly symmetric. In Fig. 4 *A* two diagrams are shown for a perfectly symmetric molecular balance, where the binding potential for the reference bond and the sample bond is identical along the pulling direction ($k_{R0} = k_{S0} = 2.82 \times 10^{-14}\ s^{-1}$ and $\Delta x_R = \Delta x_S = 2.8$ nm). For simplicity, a triangular potential was assumed based on the Bell-Evans model. On the left, the normalized binding potential $\Delta E/\Delta G_R$ is depicted for different normalized unbinding forces f/f_R. The potentials of the reference bond (*hidden blue line*) and the sample bond (*red line*) are deformed to the same degree (*left*) and no shift in the survival probability Φ_S is observed in the probability diagram (*right*).

Asymmetry in $k_{R0,S0}$

In this case, a difference in $k_{R0,S0}$ was introduced into the sample bond by lowering the transition state by 1 k_BT ($k_{S0} = 8.46 \times 10^{-14}\ s^{-1}$) while the reference bond was not changed at all ($k_{R0} < k_{S0}$), but leaving the potential width equal ($\Delta x_R = \Delta x_S$). As shown for the potentials in Fig. 4 *B* (*left*), the red and the blue lines are shifted to each other, indicating the asymmetry between the two bonds (*right*). As for the symmetric case in Fig. 4 *A*, the system is not affected in terms of the rupture probabilities by a change in loading rate, since both binding potentials are tilted by the same energy $f \times \Delta x_R = f \times \Delta x_S$.

Asymmetry in $\Delta x_{R,S}$

Here the potential width of the reference bond was chosen to be wider than the sample bond ($\Delta x_R > \Delta x_S$, $\Delta x_S = 2.66$ nm) while the potential depths were kept equal ($k_{R0} = k_{S0}$). As demonstrated in Fig. 4 *C* (*right*), the asymmetry in $\Delta x_{R,S}$ results in a pronounced dependence of the unbinding process on the force rate. Since the sample bond has a smaller Δx_S, larger rupture probabilities than for the reference bond are observed. As a consequence, the survival probability of the sample bond Φ_S (*red line*, *right*) converges toward 1 for high loading rates.

Combined asymmetry

Finally in Fig. 4 *D* an example for the combination of asymmetries in potential widths ($\Delta x_S = 2.66$ nm, $\Delta x_R > \Delta x_S$) and depths ($k_{S0} = 8.46 \times 10^{-14}\ s^{-1}$, $k_{R0} < k_{S0}$) is presented. As evidenced in the probability diagram, the sample bond is weaker then the reference bond at zero force ($f = 0$) and for small loading rates. However, at higher loading rates the disadvantage due to the larger k_{S0} is successively compensated by the advantage of a shorter Δx_S. After the red line in the right graph has crossed the 0.5 line (between rupture forces f_2 and f_3) again, an asymptotic increase toward 1 is observed.

Experiments

The theoretical concept presented above was corroborated with experiments on short oligonucleotide duplexes as previously published (22) with the goal to derive Δx_S values for several mutations in the sample duplex. With the data available in the literature (17), the assumption of triangular potentials for the reference and the sample complex are made as shown in Fig. 4, *A–D*.

For the simulation, the following input parameters are required:

1. The survival probabilities of the sample bond Φ_S, which are calculated from the fluorescence intensities as described in Materials and Methods and listed in Table 2.
2. The velocity v by which the molecules are probed is assumed to be identical to the pulling velocity.
3. The loading rate and the corresponding rupture force were simulated from k_{R0}, Δx_R, and the velocity v as described in Materials and Methods. Based on the pulling velocity of $v = 5$ nm/s, the loading rate equals 37 pN/s at a rupture force of 48 pN.
4. Natural dissociation rates $k_{R0,S0}$ at zero force for the reference duplex and the sample duplex were calculated from $\Delta G_{R,S}$ values as described in Materials and Methods.
5. The potential width of the reference bond Δx_R was derived from Strunz et al. (17), which is 2.8 nm.

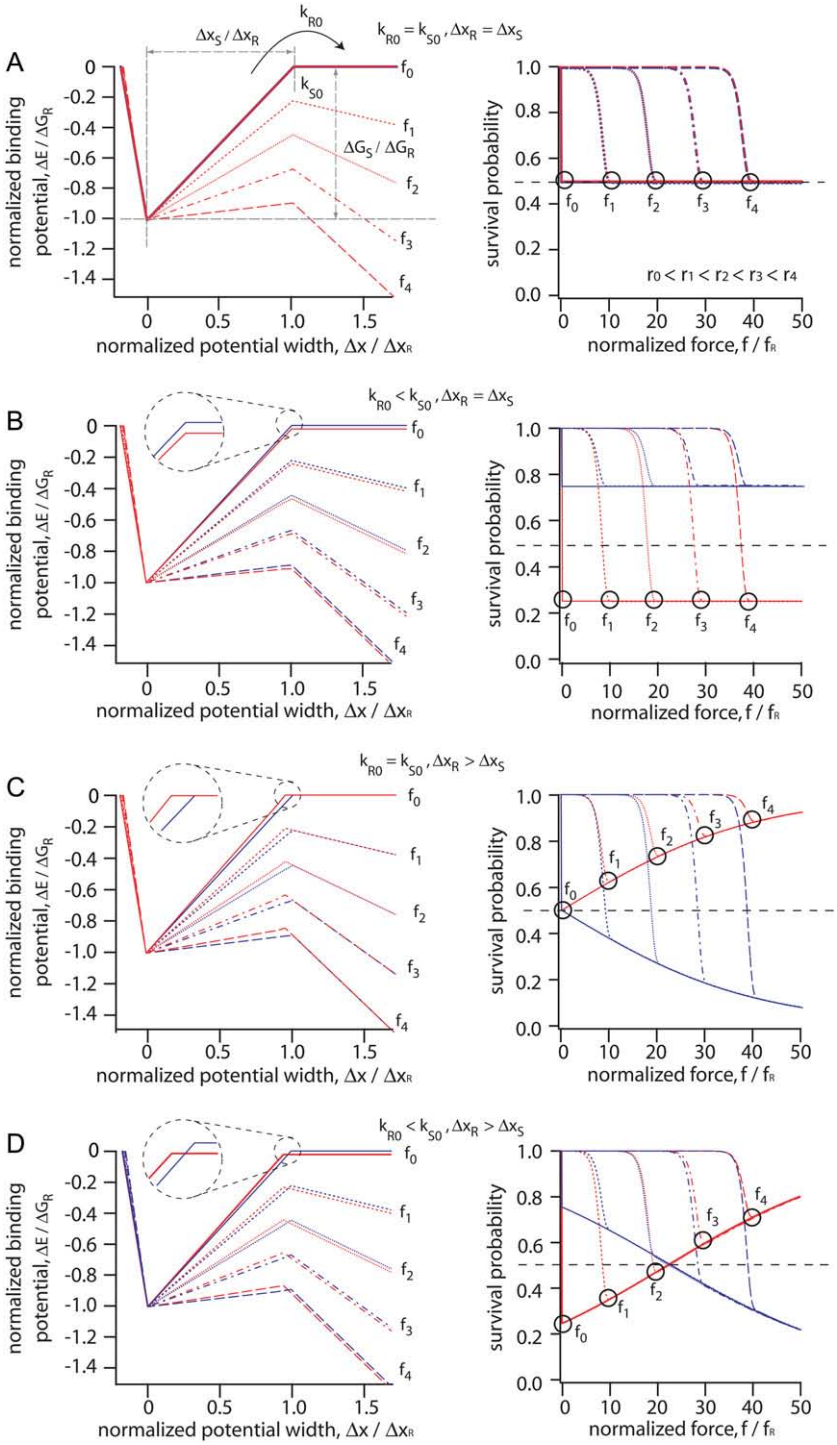

FIGURE 4 Influence of the shape of triangular binding potentials for two bonds in series. The two binding potentials of the reference (*blue*) and the sample (*red*) bond are plotted on left. The differences in potential width and depth are magnified in the inserts. The resulting survival probabilities of the two bonds are plotted on the right side. The loading rates are $r_0 = 0$ pN/s, $r_1 = 4 \times 10^{-9}$ pN/s, $r_2 = 1.5 \times 10^{-4}$ pN/s, $r_3 = 4$ pN/s, and $r_4 = 1 \times 10^5$ pN/s. The applied forces are $f_0 = 0$ pN, $f_1 = 10 \times f_R$, $f_2 = 20 \times f_R$, $f_3 = 30 \times f_R$, and $f_4 = 40 \times f_R$ with $f_R = k_B T/\Delta x_R = 1.48$ pN. (*A*) Perfectly symmetric molecular balance with identical potential width $\Delta x_{R,S} = 2.8$ nm and natural dissociation rates $k_{R0,S0} = 2.82 \times 10^{-14}$ s^{-1}. Black circles indicate the survival probability for the sample bond (*red curves*) for a given loading rate $r_{0,1,2,3,4}$ and rupture force $f_{0,1,2,3,4}$. (*B*) Asymmetry in potential depth, which corresponds to an asymmetry in $k_{R0,S0}$ for a molecular balance with identical $\Delta x_{R,S}$ but different $k_{S0} = 8.46 \times 10^{-14}$ s^{-1}. The survival probability of the sample bonds indicated by the black circles is the same for different loading rates $r_{0,1,2,3,4}$ and rupture forces $f_{0,1,2,3,4}$. (*C*) Asymmetry in $\Delta x_{R,S}$ with identical $k_{R0,S0}$ but different $\Delta x_S = 2.66$ nm. The survival probability of the sample bonds, indicated by the black circles, rises with higher loading rates and rupture forces. (*D*) Mixed asymmetry with differences in $k_{R0,S0}$ ($k_{R0} = 2.82 \times 10^{-14}$ s^{-1}, $k_{S0} = 8.46 \times 10^{-14}$ s^{-1}) and $\Delta x_{R,S}$ ($\Delta x_R = 2.8$ nm, $\Delta x_S = 2.66$ nm). The sample bonds (*red curve*) have a lower survival probability than the reference bonds (*blue curve*) for low loading rates but rises with higher loading rates and rupture forces. The crossover occurs at a rate of $r_c = 9 \times 10^{-4}$ pN/s.

For the simulation, the above-mentioned variables were kept constant and only Δx_S was varied until the minima of the curves matched the measured Φ_S values (compare to Fig. 4 and Fig. 5 *A*). Then the corresponding potential width Δx_S was extracted.

The probability diagrams for all sample duplexes are plotted in Fig. 5 *A*, showing experimental data (*light shaded bars*) for the perfect match as well as the 30GG, 30CC, and the 29CC mismatches. To get an impression about the correlation between the rupture probability and the dissociation rate k_{S0}, the measured survival probability of the sample bond Φ_S was plotted in Fig. 5 *A* over the normalized natural dissociation rate k_{S0}/k_{R0}. To calculate survival probabilities of the sample bond (shown as *solid line*), only the potential width of the sample bond was varied. The resulting normalized potential width $\Delta x_S/\Delta x_R$ is plotted in Fig. 5 *B*

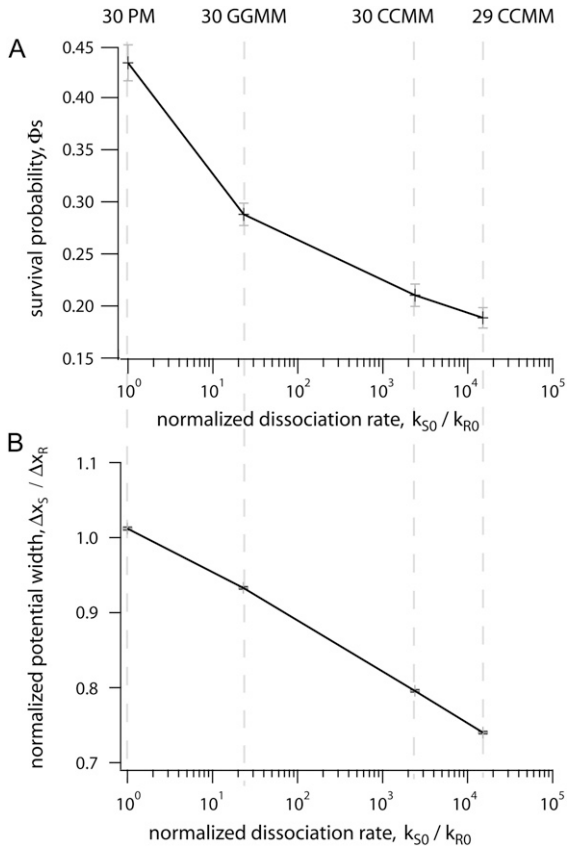

FIGURE 5 Combined data from different experiments (*light shaded bars*) and simulations (*solid line*) on a 30-mer PM, 30-mer GG MM, 30-mer CC MM, and a 29-mer CC MM. (*A*) Survival property of the sample duplex Φ_S plotted as a function of normalized dissociation rate k_{S0}/k_{R0} on a log scale. (*B*) Calculated normalized potential width of the sample duplex $\Delta x_S/\Delta x_R$ is plotted as a function of the corresponding normalized dissociation rate of the sample duplex k_{S0}/k_{R0} that matches the survival probabilities in panel *A*. The pulling velocity was $v = 5$ nm/s, resulting in a loading rate of 37 pN/s at a rupture force of 48 pN.

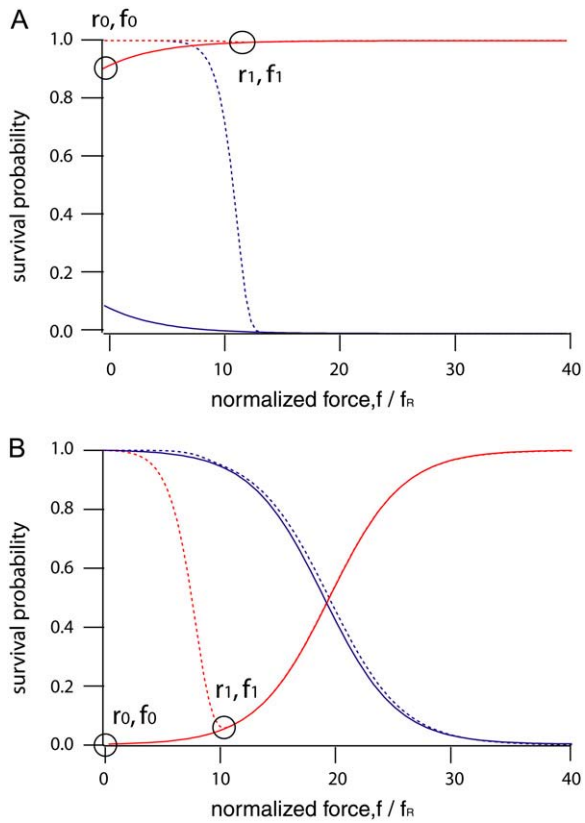

FIGURE 6 Simulation of possible AFM experiments using two bonds in series. The reference bond is a 15-bp DNA duplex (*blue*), which was immobilized by (*A*) streptavidin/biotin (*red*) and (*B*) anti-digoxigenin/digoxigenin (*red*). Black circles indicate survival probability of the immobilization tag at $f_1 = 23$ pN and $r_1 = 37$ pN/s (*dotted curves*). The black circle on the solid line indicates survival probabilities at zero force (f_0) and loading rate (r_0). Reference: $k_{R0} = 3.16 \times 10^{-5}\ s^{-1}$ and $\Delta x_R = 1.75$ nm for 15 bp DNA (17). Sample: (*A*) $k_{S0} = 3.71 \times 10^{-6}\ s^{-1}$ and $\Delta x_S = 1.31$ nm for streptavidin/biotin (41). (*B*) $k_{S0} = 0.015\ s^{-1}$ and $\Delta x_S = 1.15$ nm for anti-digoxigenin/digoxigenin (16).

as a function of the normalized natural dissociation rate of the sample complex k_{S0}/k_{R0}.

Table 2 summarizes the input parameters for all sample duplexes and the reference duplex. The $\Delta x_{R,S}$ values are also listed, calculated by using the differential equation Eqs. 7A–7C (with exception of $\Delta x_{R,S}$ for the 30-bp perfect match, which was taken from the data provided in (17)).

Besides the analysis of force-balance measurements, our simulations are useful for designing force experiments where the sample is bound to a surface by a receptor ligand immobilization tag. In Fig. 6, two simulations of AFM experiments are depicted, where streptavidin/biotin (Fig. 6 *A*) and anti–digoxigenin/digoxigenin (Fig. 6 *B*), respectively, are used to immobilize a 15-bp DNA duplex. Again, survival probabilities for the DNA (*blue*) and for the immobilization tag (*red*) are plotted as function of the normalized force for different loading rates. Here, the reference duplex is a 15-bp DNA duplex with a natural dissociation rate of $k_{R0} = 3.16 \times 10^{-5}\ s^{-1}$, a potential width of $\Delta x_R = 1.75$ nm, and a characteristic force $f_R = 2.36$ pN. For a loading rate of 37 pN/s, the survival probability of the immobilization tag (*red*) is highlighted by a black circle. It is evident from Fig. 6 *A*, which the streptavidin survives over the whole force range with a likelihood of >99%. In contrast, the antibody bond is not sufficiently strong for the experiment and would fail with a probability of ~90%.

DISCUSSION

We can proceed from the assumption that for a molecular force balance, which is perfectly symmetric in terms of $k_{R0,S0}$ and $\Delta x_{R,S}$, the relative rupture probability is independent of any changes in pulling velocity and loading rate (Fig. 4 *A*). However, even small variations of the sample duplex binding potential breaks the symmetry and gives rise to significant differences in survival probability as illustrated by Fig. 4, *B* and *C*. Compared to the fully symmetric balance in

4 *A*, where both the reference and the sample bond survival probabilities converge toward 0.5, a huge shift is observed when ΔG_S and Δx_S of the sample bond are changed just between 2 and 5% compared to the reference bond. Interestingly, for changes in k_{S0}, Φ_S stays constant over the entire loading range, while for changes in Δx_S, Φ_S varies with an increase of the applied loading rate.

As shown by Strunz et al. (17), deletions of peripheral basepairs from a 30-bp DNA duplex give rise to decreasing k_{S0} and increasing Δx_S. Since the deletion affects both variables in the opposite direction, it is evident that a substantial part of the lowering in binding energy is compensated by a decrease in Δx_S when we consider the resulting survival probabilities. This is illustrated by Fig. 4 *D* where a case with differences in $k_{R0,S0}$ and $\Delta x_{R,S}$ was simulated. It is evident from the red line that the drop in the survival probability of the sample complex Φ_S becomes smaller for increasing loading rates, since the difference in $\Delta x_{R,S}$ causes an asymptotic rise, which compensates the differences between k_{R0} and k_{S0}.

In contrast to DNA duplexes, no such correlation was generally expected for an antibody antigen system like that investigated by Schwesinger et al. (18). There the effect of single amino-acid exchanges in the binding pocket of antihapten single-chain fragment antibodies was analyzed by AFM force spectroscopy. Since the mutations should not have altered the geometry of the binding pocket, $\Delta x_{R,S}$ was assumed to be constant despite changes in the binding energy. Surprisingly, the antibody system shows a qualitatively similar behavior as the DNA duplexes studied by Strunz. Again, a linear correlation between the logarithm of the natural dissociation rate k_{S0} and the potential width Δx_S was found as shown in Fig. 5 *A*.

For the experiments presented here, we have introduced internal basepair mismatches to the DNA duplex, because such mutations have about the half effect on ΔG_S compared to a 10-bp deletion (17), but without affecting the contour length of the duplex. Therefore, we expected the effect of the mutations on Δx_S to be rather small compared to the 10-bp deletions.

To facilitate a quantitative comparison of our data to that of Strunz et al. (17), we calculated $\Delta G_{R,S}$ values based on the nearest-neighbor algorithm as explained above for both experiments. In Fig. 5 *B*, the normalized potential width $\Delta x_S/\Delta x_R$ over normalized dissociation rate k_{S0}/k_{R0} is plotted, and in accordance to the procedure from Schwesinger et al. (18), we obtained a slope for the Strunz data of 0.53 (17) close to the value measured by Schwesinger for the single-chain fragment antibodies of 0.3. In contrast to that, our point mutations resulted in an even higher slope of 0.8. In other words, a single-point mutation like the CC homoduplex accounts for a difference in ΔG_S comparable to an 8-bp deletion (7.8 k_BT) but equals a shift in Δx_S comparable to a 10-bp deletion according to the equation from Strunz. Hence, the compensation of ΔG_S (k_{S0}) by Δx_S in terms of the resulting survival probability Φ_S is more pronounced for internal mismatches than for peripheral deletions in DNA. This may be an explanation for the fact that discrimination of mismatches has not been reported for the AFM so far, in contrast to energetically comparable peripheral deletions (17).

As seen in Fig. 5, the experimental data are reproduced very well using the approximation of triangular potentials for the reference and the sample complex (17). Furthermore, this framework of comparing two bonds in series is also extendible to other potential shapes. If the reference potential is known in better detail, a wide range of loading rates can be measured, because only the differences between the potentials of the reference and the sample complexes are measured. And even if these differences are small, this method has the potential to resolve them.

There are some potential challenges in applying this technique directly to molecular interactions when the spontaneous dissociation rates become comparable to the timescale of the experiment. If the sample and the reference complex are too weak, they start to dissociate even during assembly of the assay. The consequence will be a change of concentrations of reference and sample complex during the experiment without applying a force. But if one uses the experimental setup above to measure the interactions of molecules that bind to just the sample DNA, in principle it is also possible to measure weaker interactions. These interactions act only on the sample complex in the time frame of the contact of the stamp with the slide and not during the assembly of the assay.

In addition to analyzing force-balance experiments, the theoretical model also was applied to prove the suitability of immobilization tags for force experiments, as illustrated in Fig. 6. The fact that streptavidin/biotin (Fig. 6 *A*) is very well suited for immobilization of samples under force is again corroborated by the simulation for forces at least up to 100 pN. In contrast to that, it is critical to rely on a single digoxigenin/antibody bond, which fails for low loading rates in comparison to a 15-mer DNA (Fig. 6 *B*).

Furthermore, it is evident that DNA duplexes may be used as reference bonds to determine the k_{S0} and Δx_S values of protein receptors like the anti-digoxigenin antibody. However, for the streptavidin/biotin bond it would be hard to find a matching DNA duplex, since the rupture force of 15 bp is much too low and even much longer DNA double strands will not exceed the 65 pN barrier of the BS-transition (39,40).

We thank Robert Lugmaier, Julia Morfill, Kay Gottschalk, Dominik Ho, Katja Falter, and Erich Sackmann for helpful discussions.

This work was supported by the Deutsche Forschungsgemeinschaft.

REFERENCES

1. Rief, M., M. Gautel, F. Oesterhelt, J. M. Fernandez, and H. E. Gaub. 1997. Reversible unfolding of individual titin immunoglobulin domains by AFM. *Science.* 276:1109–1112.

2. Rief, M., F. Oesterhelt, B. Heymann, and H. E. Gaub. 1997. Single molecule force spectroscopy on polysaccharides by atomic force microscopy. *Science*. 275:1295–1297.
3. Grandbois, M., M. Beyer, M. Rief, H. Clausen-Schaumann, and H. E. Gaub. 1999. How strong is a covalent bond? *Science*. 283:1727–1730.
4. Hugel, T., and M. Seitz. 2001. The study of molecular interactions by AFM force spectroscopy. *Macromol. Rapid Commun.* 22:989–1016.
5. Hugel, T., N. B. Holland, A. Cattani, L. Moroder, M. Seitz, and H. E. Gaub. 2002. Single-molecule optomechanical cycle. *Science*. 296: 1103–1106.
6. Bustamante, C. 2005. Unfolding single RNA molecules: bridging the gap between equilibrium and non-equilibrium statistical thermodynamics. *Q. Rev. Biophys.* 38:291–301.
7. Bockelmann, U. 2004. Single-molecule manipulation of nucleic acids. *Curr. Opin. Struct. Biol.* 14:368–373.
8. Charvin, G., T. R. Strick, D. Bensimon, and V. Croquette. 2005. Tracking topoisomerase activity at the single-molecule level. *Annu. Rev. Biophys. Biomol. Struct.* 34:201–219.
9. Gore, J., Z. Bryant, M. Nollmann, M. U. Le, N. R. Cozzarelli, and C. Bustamante. 2006. DNA overwinds when stretched. *Nature*. 442: 836–839.
10. Evans, E. 1998. Energy landscapes of biomolecular adhesion and receptor anchoring at interfaces explored with dynamic force spectroscopy. *Faraday Discuss.* 111:1–16.
11. Merkel, R. 2001. Force spectroscopy on single passive biomolecules and single biomolecular bonds. *Phys. Rep. Rev. Phys. Lett.* 346:344–385.
12. Holland, N. B., T. Hugel, G. Neuert, A. Cattani-Scholz, C. Renner, D. Oesterhelt, L. Moroder, M. Seitz, and H. E. Gaub. 2003. Single molecule force spectroscopy of azobenzene polymers: switching elasticity of single photochromic macromolecules. *Macromolecules.* 36:2015–2023.
13. Neuert, G., T. Hugel, R. R. Netz, and H. E. Gaub. 2006. Elasticity of poly(azobenzene-peptides). *Macromolecules.* 39:789–797.
14. Bell, G. I. 1978. Models for the specific adhesion of cells to cells. *Science*. 200:618–627.
15. Merkel, R., P. Nassoy, A. Leung, K. Ritchie, and E. Evans. 1999. Energy landscapes of receptor-ligand bonds explored with dynamic force spectroscopy. *Nature*. 397:50–53.
16. Neuert, G., C. Albrecht, E. Pamir, and H. E. Gaub. 2006. Dynamic force spectroscopy of the digoxigenin-antibody complex. *FEBS Lett.* 580:505–509.
17. Strunz, T., K. Oroszlan, R. Schafer, and H. J. Guntherodt. 1999. Dynamic force spectroscopy of single DNA molecules. *Proc. Natl. Acad. Sci. USA*. 96:11277–11282.
18. Schwesinger, F., R. Ros, T. Strunz, D. Anselmetti, H. J. Guntherodt, A. Honegger, L. Jermutus, L. Tiefenauer, and A. Pluckthun. 2000. Unbinding forces of single antibody-antigen complexes correlate with their thermal dissociation rates. *Proc. Natl. Acad. Sci. USA*. 97: 9972–9977.
19. Nishizaka, T., H. Miyata, H. Yoshikawa, S. Ishiwata, and K. Kinosita. 1995. Unbinding force of a single motor molecule of muscle measured using optical tweezers. *Nature*. 377:251–254.
20. Lang, M. J., P. M. Fordyce, A. M. Engh, K. C. Neuman, and S. M. Block. 2004. Simultaneous, coincident optical trapping and single-molecule fluorescence. *Nat. Methods*. 1:133–139.
21. Albrecht, C., K. Blank, M. Lalic-Multhaler, S. Hirler, T. Mai, I. Gilbert, S. Schiffmann, T. Bayer, H. Clausen-Schaumann, and H. E. Gaub. 2003. DNA: a programmable force sensor. *Science*. 301: 367–370.
22. Albrecht, C. H., H. Clausen-Schaumann, and H. E. Gaub. 2006. Differential analysis of biomolecular rupture forces. *J. Phys. Condens. Matter*. 18:S581–S599.
23. Blank, K., A. Lankenau, T. Mai, S. Schiffmann, I. Gilbert, S. Hirler, C. Albrecht, M. Benoit, H. E. Gaub, and H. Clausen-Schaumann. 2004. Double-chip protein arrays: force-based multiplex sandwich immunoassays with increased specificity. *Anal. Bioanal. Chem.* 379:974–981.
24. Blank, K., T. Mai, I. Gilbert, S. Schiffmann, J. Rankl, R. Zivin, C. Tackney, T. Nicolaus, K. Spinnler, F. Oesterhelt, M. Benoit, H. Clausen-Schaumann, and H. E. Gaub. 2003. A force-based protein biochip. *Proc. Natl. Acad. Sci. USA*. 100:11356–11360.
25. Gilbert, L., S. Schiffmann, S. Rubenwolf, K. Jensen, T. Mail, C. Albrecht, A. Lankenau, G. Beste, K. Blank, H. E. Gaub, and H. Clausen-Schaumann. 2004. Double chip protein arrays using recombinant single-chain Fv antibody fragments. *Proteomics*. 4:1417–1420.
26. Evans, E., and K. Ritchie. 1997. Dynamic strength of molecular adhesion bonds. *Biophys. J.* 72:1541–1555.
27. Evans, E., and K. Ritchie. 1999. Strength of a weak bond connecting flexible polymer chains. *Biophys. J.* 76:2439–2447.
28. Friedsam, C., A. K. Wehle, F. Kühner, and H. E. Gaub. 2003. Dynamic single-molecule force spectroscopy: bond rupture analysis with variable spacer length. *J. Phys. Condens. Matter*. 15:S1709–S1723.
29. Allemand, J. F., D. Bensimon, and V. Croquette. 2003. Stretching DNA and RNA to probe their interactions with proteins. *Curr. Opin. Struct. Biol.* 13:266–274.
30. Berquand, A., N. Xia, D. G. Castner, B. H. Clare, N. L. Abbott, V. Dupres, Y. Adriaensen, and Y. F. Dufrene. 2005. Antigen binding forces of single antilysozyme Fv fragments explored by atomic force microscopy. *Langmuir*. 21:5517–5523.
31. Evans, E. 2001. Probing the relation between force lifetime and chemistry in single molecular bonds. *Annu. Rev. Biophys. Biomol. Struct.* 30:105–128.
32. Gore, J., Z. Bryant, M. D. Stone, M. Nollmann, N. R. Cozzarelli, and C. Bustamante. 2006. Mechanochemical analysis of DNA gyrase using rotor bead tracking. *Nature*. 439:100–104.
33. Hinterdorfer, P., and Y. F. Dufrene. 2006. Detection and localization of single molecular recognition events using atomic force microscopy. *Nat. Methods*. 3:347–355.
34. Williams, M. C., and I. Rouzina. 2002. Force spectroscopy of single DNA and RNA molecules. *Curr. Opin. Struct. Biol.* 12:330–336.
35. Reference deleted in proof.
36. SantaLucia, J., Jr. 1998. A unified view of polymer, dumbbell, and oligonucleotide DNA nearest-neighbor thermodynamics. *Proc. Natl. Acad. Sci. USA*. 95:1460–1465.
37. Peyret, N., P. A. Seneviratne, H. T. Allawi, and J. SantaLucia, Jr. 1999. Nearest-neighbor thermodynamics and NMR of DNA sequences with internal A·A, C·C, G·G, and T·T mismatches. *Biochemistry*. 38:3468–3477.
38. Northrup, S. H., and H. P. Erickson. 1992. Kinetics of protein-protein association explained by Brownian dynamics computer simulation. *Proc. Natl. Acad. Sci. USA*. 89:3338–3342.
39. Smith, S. B., Y. J. Cui, and C. Bustamante. 1996. Overstretching B-DNA: the elastic response of individual double-stranded and single-stranded DNA molecules. *Science*. 271:795–799.
40. Cluzel, P., A. Lebrun, C. Heller, R. Lavery, J. L. Viovy, D. Chatenay, and F. Caron. 1996. DNA: an extensible molecule. *Science*. 271: 792–794.
41. Pincet, F., and J. Husson. 2005. The solution to the streptavidin-biotin paradox: the influence of history on the strength of single molecular bonds. *Biophys. J.* 89:4374–4381.